Tao Wang et al. (2022) The role of visual sensor-based CT imaging for rapid diagnosis of lung cancer markers in athletic patients.Revista Internacional de Medicina y Ciencias de la Actividad Física y el Deporte vol. 22 (88.1) pp. 318-335
DOI: https://doi.org/10.15366/rimcafd2022.88.1.023

ORIGINAL

The role of visual sensor-based CT imaging for rapid diagnosis of lung cancer markers in athletic patients

Bin Li[1], Meiju Gao[2], Tao Wang[, *]

[1] Lüliang People's Hospital, Lvliang,033000, China
[2] Qingdao Eighth People 's Hospital, Qingdao,266100, China
[3] Fourth People's Hospital of Sichuan Province, Chengdu,610016, China

*Corresponding author: Tao Wang
E-mail: chnwangtao@163.com

UNESCO Code / UNESCO Code:
Council of Europe classification / Council of Europe classification:

Recibido 30 de abril de 2021 **Received** April 30, 2021
Aceptado 26 de junio de 2021 **Accepted** June 26, 2022

ABSTRACT

Lung cancer has the greatest fatality rate, requiring a biopsy to confirm its subtype before therapy can begin. Deep learning has recently developed significant tools for lung cancer diagnosis and treatment planning in athletic patients. In any case, diagnosing the neurotic sort of cellular breakdown in the lungs in its beginning phases utilizing CT pictures stays troublesome because of an absence of accessible preparing information and incredible counterfeit shrewd models. The wide range of diagnoses makes a precise prediction and subtype classification of lung cancer in athletic patients critical. Pathologists now use Computer Aided Diagnosis (CAD) to make accurate diagnoses. Our research shows how to use a pre-trained Deep Convolutional Neural Networks (DCNN) architecture called Visual Geometry Group – 16 (VGG16) to detect, predict, and categorize ovarian cancer in athletic patient's subtypes from histopathology pictures. VGG-16 comprises of 16 layers (13 convolution layers, three completely associated layers, five max-pooling layers, and one softmax layer). For this examination, we obtained 1000 CT filter pictures of lungs in four gatherings (adenocarcinoma, huge cell carcinoma, squamous cell carcinoma and ordinary). By using just 613 CT scan images our model can detect and classify lung cancer with having an accuracy of 77.61% in less than 2 seconds which is higher that accuracy of manual detection as the dataset increases more accurate our model became which shows us a possible way for more accurate and fast cancer detection.

KEYWORDS: Lung Cancer, convoluted Neural Network, VGG16 architecture, cancer detection

INTRODUCTION

Cell breakdown in the lungs is as of now one of the most generally perceived explanations behind harmful development-related end in individuals. As a result, competent radiologists are required to accurately identify lung cancer in its early stages

to prevent human mortality. As a result, detecting lung nodules that are influenced by cancer or non-cancer in their early stages is difficult. Cell breakdown in the lungs is one of the primary wellsprings of death, with various individuals failing miserably each year from this terrible ailment. As a result, appropriate mechanisms for detecting and identifying this disease early on should be implemented to preserve the lives of many persons suffering from lung cancer. The survival rate of many athletic patients can be enhanced if it is diagnosed and identified in the early stages. After a condition has been identified, offering the correct diagnosis can help athletic patients live longer. So, to obtain a reasonable and instantaneous result, employing modern machine learning approaches in the medical image processing area by increasing the amount of duplication for the methods used can improve classification accuracy. As a result, quick detection and identification in the early stages of the disease will almost certainly enhance the survival level and lower the death rate. Clinical imaging has progressed in innovation, and most of the past examinations utilized registered tomography (CT), attractive reverberation imaging (MRI), and mammography pictures. Utilizing appropriate approaches, the specialist doctor in this subject analyses and identifies the various degrees of lung cancer in athletic patients using these photos. Chemical treatment to destroy or inhibit the duplications of malignant cells, targeted therapy, and radiotherapy are among the laboratory and clinical steps used.

Radiologists have been manually analyzing CT scans of the lungs in recent days, looking for prospective nodules and identifying malignant and non-cancerous cells in those nodules. This procedure necessitates a thorough understanding of lung nodules and is both difficult and time-consuming. Subsequently, this can be settled by utilizing a PC supported conclusion (CAD) framework to identify lung knobs and group them as destructive or non-harmful. This device will serve as a backup to the radiologist in detecting and analyzing lung nodules. Early detection of lung cancer can improve treatment effectiveness and boost athletic patients' chances of survival. Noninvasive imaging strategies like figured tomography (CT), contrast-improved processed tomography (CE-CT), low-portion registered tomography (LDCT), and positron emanation tomography (PET) would all be able to be utilized to analyze cellular breakdown in the lungs (PET).

CAD systems have been developed in recent years for both nodule segmentation and categorization of lung nodules as malignant or non-cancerous. However, while this technique for segmentation will produce a high-quality identification of lung nodules, it will also produce a large number of false positives, with a ratio of hundreds of true positives to false positive segmentation. As a result, when it comes to lung cancer in athletic patients, this system can lead to a lot of false positives.

It is preferable to label anything in the image that appears to be a nodule, and radiologists must use manual methods to detect lung cancer in athletic patients.

Traditional image processing algorithms were employed to find distinctive features in images. As a result, handcrafted features must be built, which learns features through a laborious approach. As a result, distinguishing between malignant and non-cancerous nodules using this method is extremely difficult. As a result, deep learning may avoid all of these issues and can deal with issues like image identification, video recognition, speech recognition, and natural language processing, among others.

Manual feature extraction necessitates the designer's specialist knowledge of lung cancer in athletic patients. Deep learning will be able to recognize all of the features in the photographs. Convolutional Neural Network (CNN) extracts features from input

images using one or more hierarchical layers of convolution, sub sampling, or max-pooling. Convolution, Max-surveying, and completely associated are the three levels of an overall CNN. CNN performs picture categorization by extracting characteristics from each layer and generating a final model. When a second test image is provided, the model compares the features of the two and assigns the photos to different classes based on their accuracy.

Methodology

To detect lung cancer using CT scan images we use deep CNN algorithms using VGG16 architecture in athletic patients

DATASET

To fit the model, pictures are in jpg or png design(Travis et al., 2010). The information incorporates three types of chest malignant growth: adenocarcinoma, enormous cell carcinoma, and squamous cell carcinoma, just as one organizer for typical cells(Siegel, Miller, & Jemal, 2015).

Information envelope is the fundamental organizer that contain all the progression organizers inside Data organizer are test , train , legitimate :

- training set is 70%
- testing set is 20%
- validation set is 10%

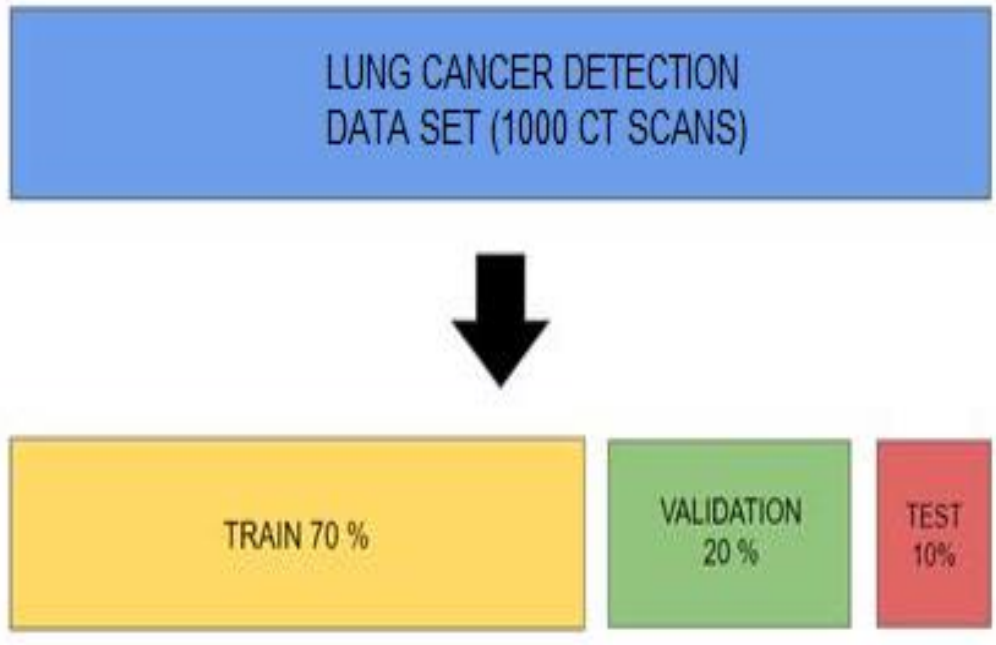

Figure 1: Representing Dataset

Adenocarcinoma

Lung adenocarcinoma: The most generally perceived sort of cell breakdown in the lungs is lung adenocarcinoma, which addresses 30% of all cases and around 40% of all non-little cell breakdown in the lungs cases(A. Wang et al., 2015). Adenocarcinomas can be

found in a grouping of cancers, including chest, prostate, and colorectal sicknesses(Nawa et al., 2012). In the external area of the lung, adenocarcinomas are found in the organs that create bodily fluid and assist us with relaxing(Barnes, Eveson, Reichart, & Sidransky, 2005). A portion of the manifestations incorporate hacking, roughness, weight reduction, and shortcoming(Kundu, Mitra, Misra, & Chatterjee, 2012).

Test

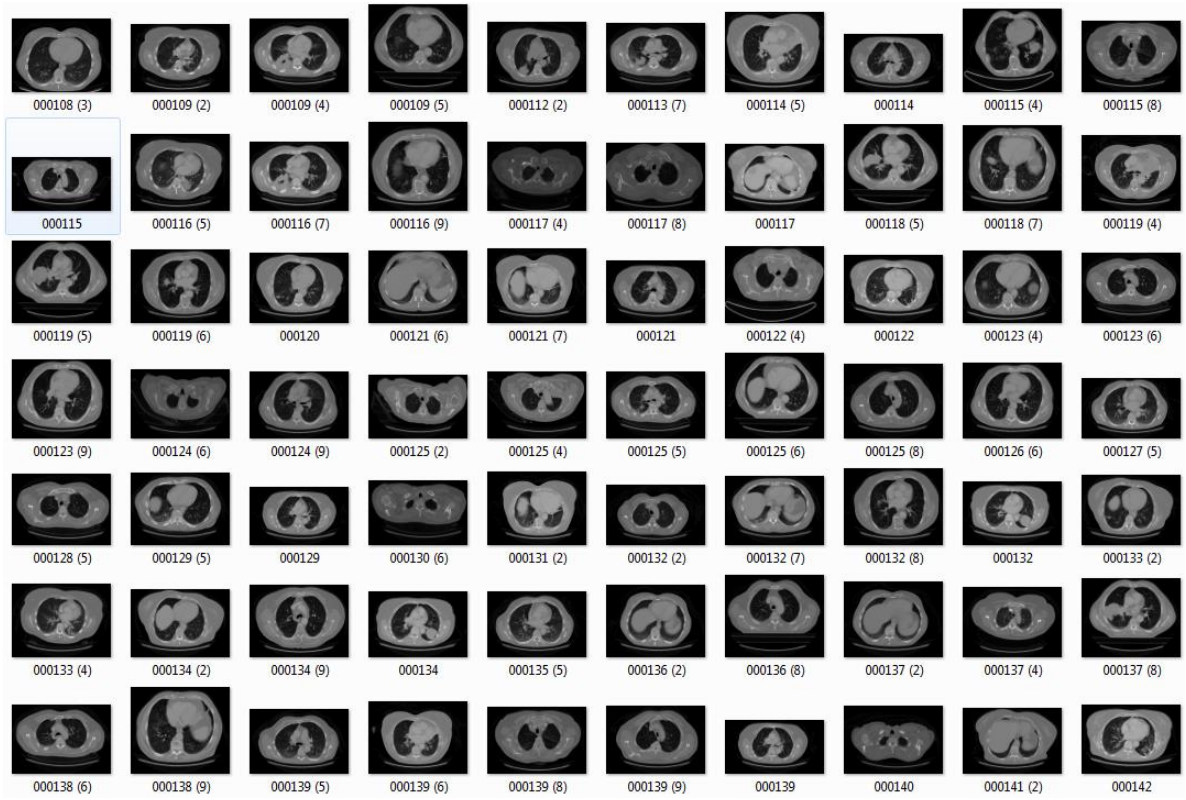

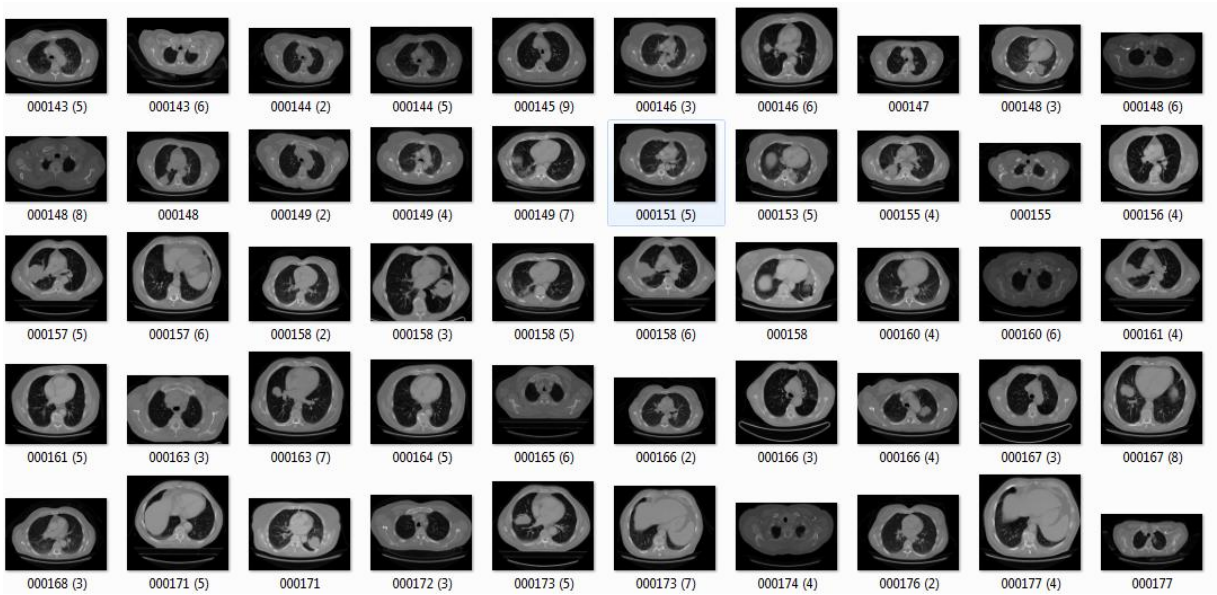

Train


000000 (6)
000005 (3)
000005 (9)
000008 (10)
000009 (3)
000009 (7)
000013 (4)
000013 (8)
000014 (7)
000015 (4)
000015 (9)
000015 (10)
000016 (9)
000017 (6)
000017 (8)
000018 (5)
000019 (5)
000020 (5)
000020 (6)
000020 (10)
000021 (3)
000021 (4)
000021 (5)
000021 (6)
000021 (8)
000022 (2)
000022 (8)
000022 (9)
000022 (10)
000022
000023 (5)
000023 (7)
000023 (9)
000023 (10)
000024 (6)
000024 (7)
000024 (10)
000024
000025 (6)
000026 (3)
000026 (10)
000027 (4)
000027 (6)
000029 (4)
000029 (5)
000029 (9)
000030 (4)
000031 (3)
000032 (8)
000033 (9)

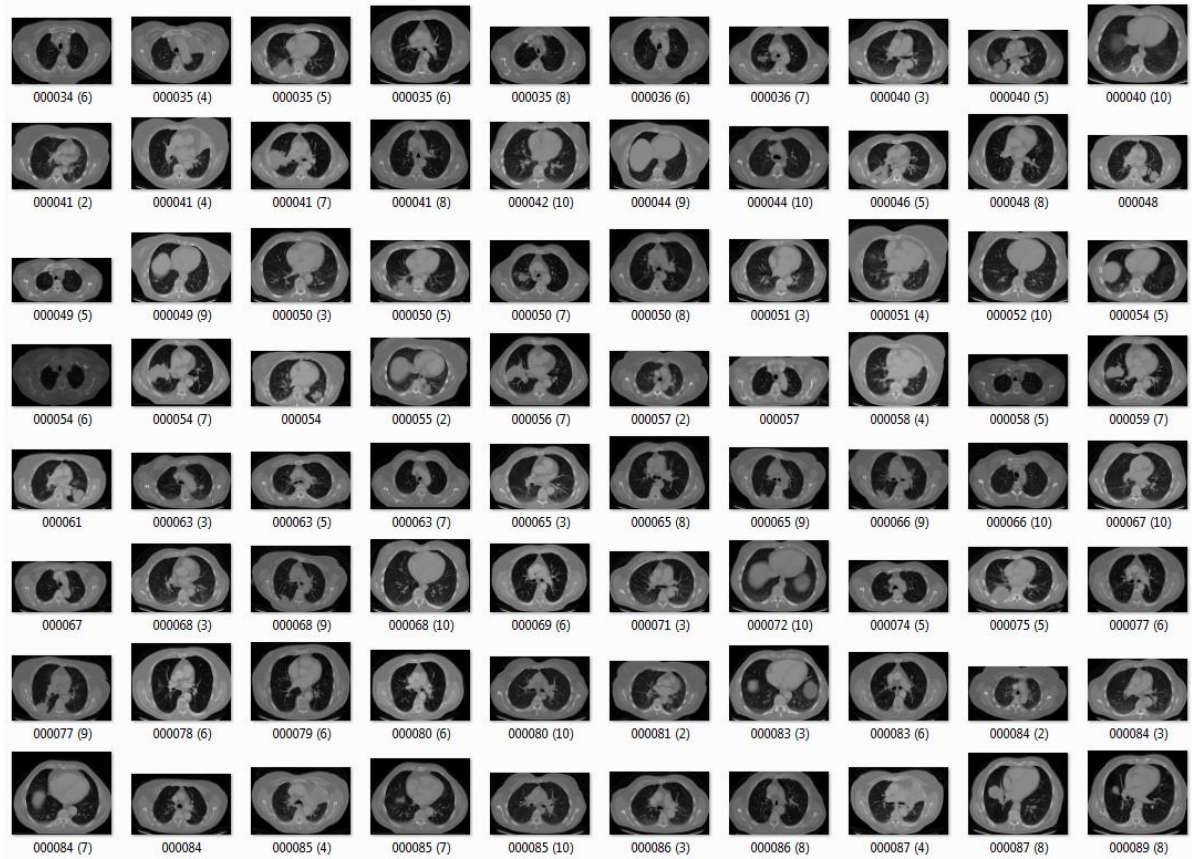
000034 (6)
000035 (4)
000035 (5)
000035 (6)
000035 (8)
000036 (6)
000036 (7)
000040 (3)
000040 (5)
000040 (10)
000041 (2)
000041 (4)
000041 (7)
000041 (8)
000042 (10)
000044 (9)
000044 (10)
000046 (5)
000048 (8)
000048
000049 (5)
000049 (9)
000050 (3)
000050 (5)
000050 (7)
000050 (8)
000051 (3)
000051 (4)
000052 (10)
000054 (5)
000054 (6)
000054 (7)
000054
000055 (2)
000056 (7)
000057 (2)
000057
000058 (4)
000058 (5)
000059 (7)
000061
000063 (3)
000063 (5)
000063 (7)
000065 (3)
000065 (8)
000065 (9)
000066 (9)
000066 (10)
000067 (10)
000067
000068 (3)
000068 (9)
000068 (10)
000069 (6)
000071 (3)
000072 (10)
000074 (5)
000075 (5)
000077 (6)
000077 (9)
000078 (6)
000079 (6)
000080 (6)
000080 (10)
000081 (2)
000083 (3)
000083 (6)
000084 (2)
000084 (3)
000084 (7)
000084
000085 (4)
000085 (7)
000085 (10)
000086 (3)
000086 (8)
000087 (4)
000087 (8)
000089 (8)

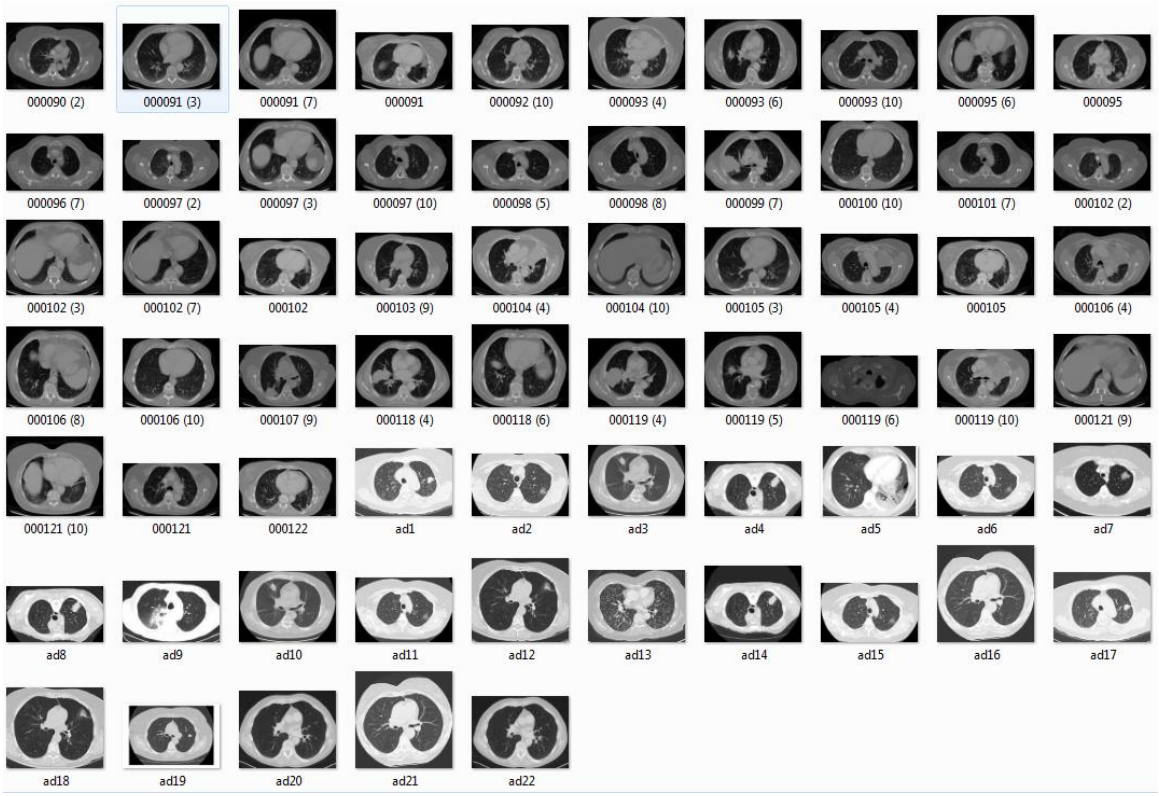

Valid

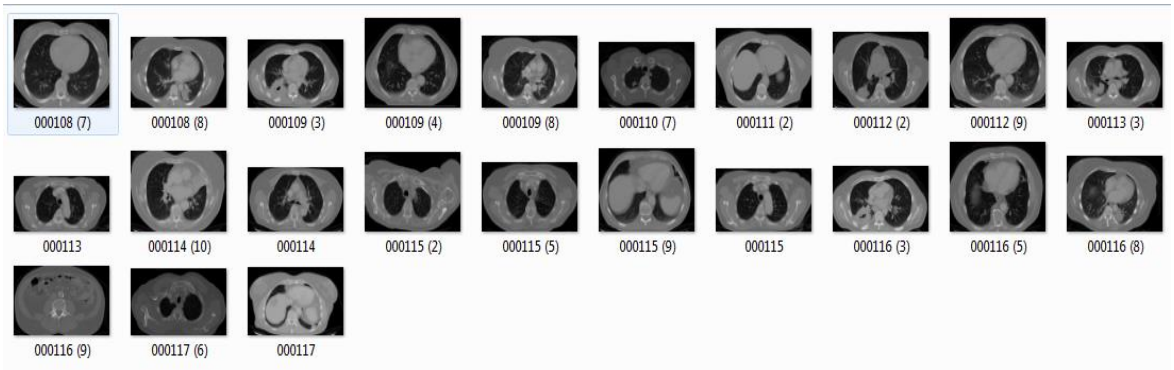

Large cell carcinoma

Cellular breakdown in the lungs that beginnings and spreads rapidly and can arise anyplace in the lungs is known as enormous cell undifferentiated carcinoma(Chang & Kundranda, 2017). This kind of cellular breakdown in the lungs represents around 10% to 15% of all NSCLC cases(Barbareschi et al., 2011).

Enormous cell undifferentiated carcinoma tends to develop and spread rapidly(Wei, Guo, Wang, & Wan, 2015)

Test


000108
000110
000111 (2)
000111
000113 (2)
000113
000114
000115 (2)
000116
000118
000120
000122
000123
000124 (2)
000126
000127 (2)
000128 (2)
000128
000130
000131 (2)
000131
000132 (2)
000133 (2)
000133
000136 (2)
000137
000138 (2)
000141
000143
000147 (2)
000148 (2)
000148
000149
000150
000154 (2)
000154
000155
000158
000159 (2)
000159
000160
000162
000163
000169
000170
000171
000172 (2)
000172
000173 (2)
000173
000174

Train

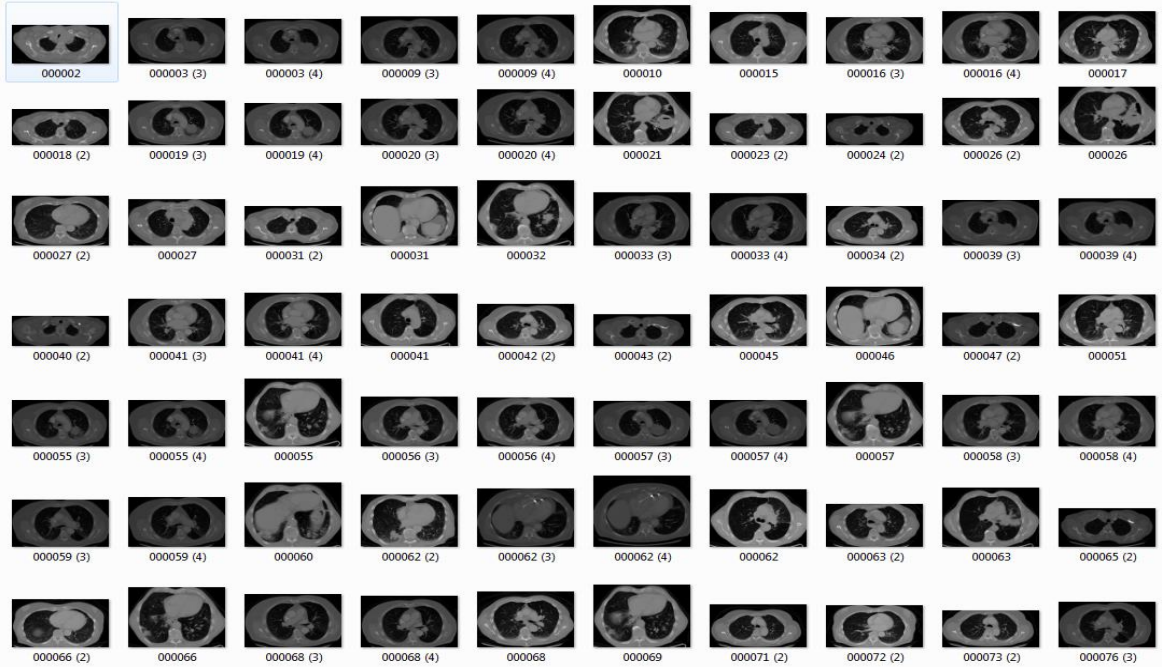
000002
000003 (3)
000003 (4)
000009 (3)
000009 (4)
000010
000015
000016 (3)
000016 (4)
000017
000018 (2)
000019 (3)
000019 (4)
000020 (3)
000020 (4)
000021
000023 (2)
000024 (2)
000026 (2)
000026
000027 (2)
000027
000031 (2)
000031
000032
000033 (3)
000033 (4)
000034 (2)
000039 (3)
000039 (4)
000040 (2)
000041 (3)
000041 (4)
000041
000042 (2)
000043 (2)
000045
000046
000047 (2)
000051
000055 (3)
000055 (4)
000055
000056 (3)
000056 (4)
000057 (3)
000057 (4)
000057
000058 (3)
000058 (4)
000059 (3)
000059 (4)
000060
000062 (2)
000062 (3)
000062 (4)
000062
000063 (2)
000063
000065 (2)
000066 (2)
000066
000068 (3)
000068 (4)
000068
000069
000071 (2)
000072 (2)
000073 (2)
000076 (3)

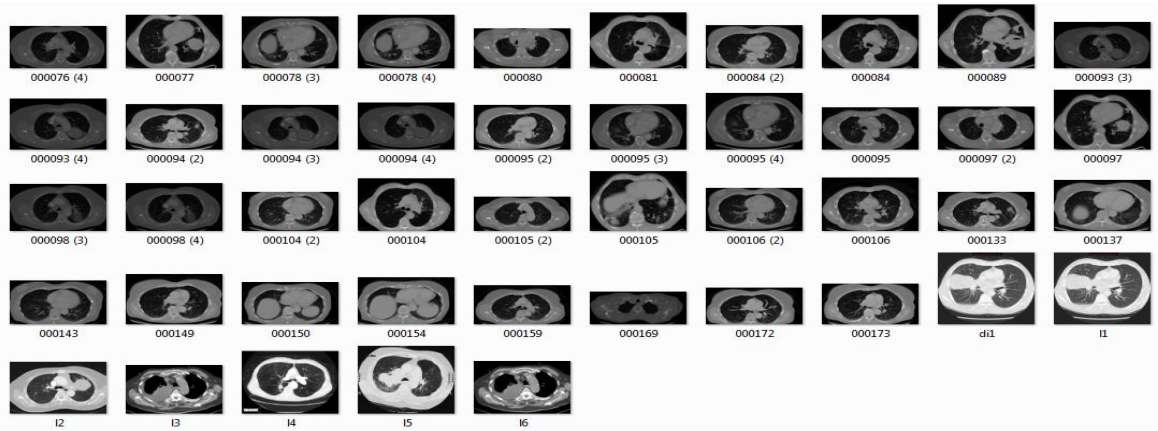

Valid

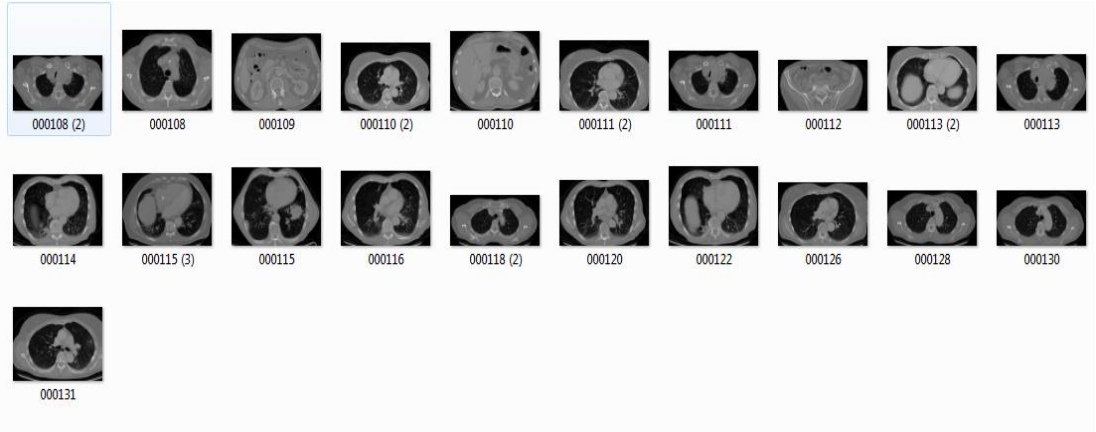

Squamous cell carcinoma

Squamous cell cellular breakdown in the lungs begins in the lung's middle, where the bigger bronchi join the windpipe and lung(Wiener, Schwartz, Woloshin, & Welch, 2011), or in one of the principle aviation route branches. Squamous cell cellular breakdown in the lungs, which makes up in excess of 33% of all non-little cell cellular breakdowns in the lungs, is habitually connected to smoking(S.-H. Wang et al., 2019).

Test

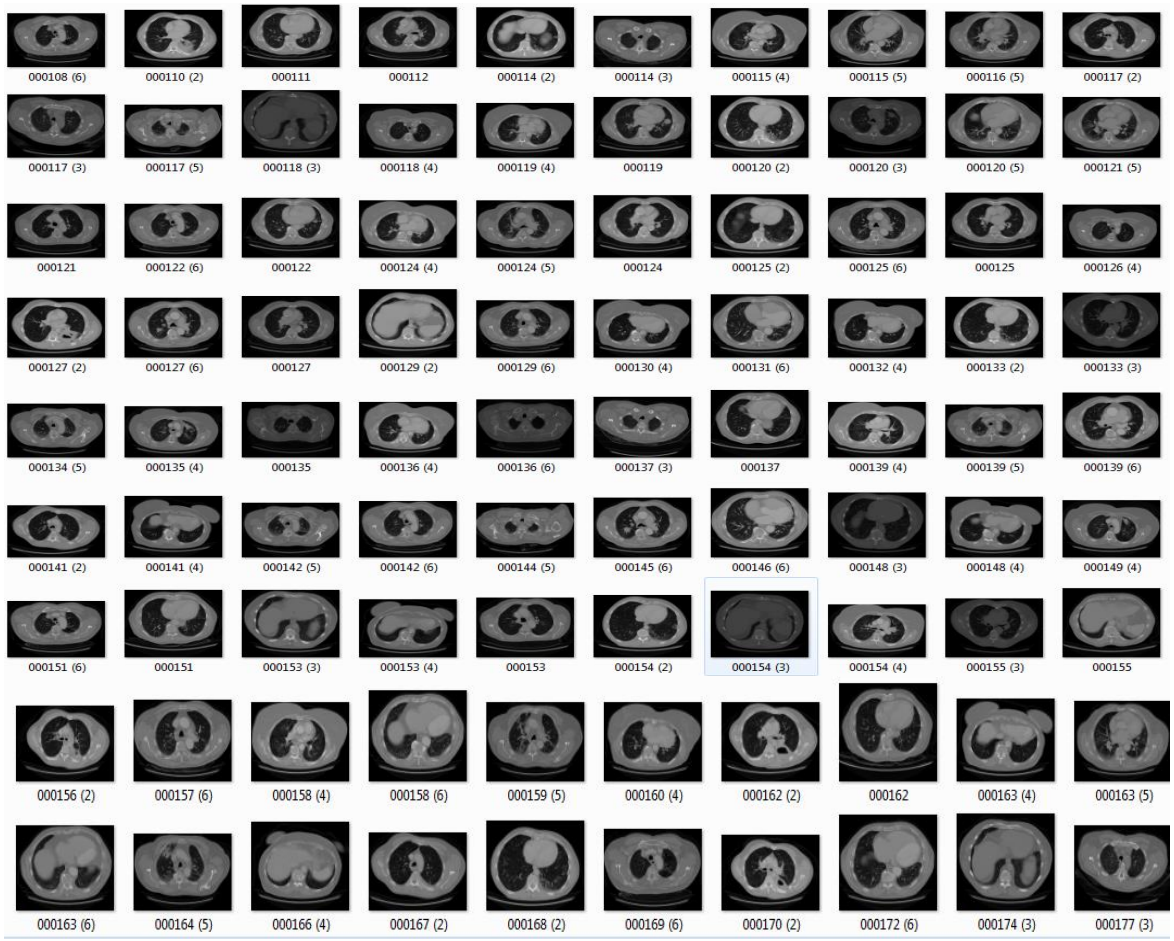
000108 (6)
000110 (2)
000111
000112
000114 (2)
000114 (3)
000115 (4)
000115 (5)
000116 (5)
000117 (2)
000117 (3)
000117 (5)
000118 (3)
000118 (4)
000119 (4)
000119
000120 (2)
000120 (3)
000120 (5)
000121 (5)
000121
000122 (6)
000122
000124 (4)
000124 (5)
000124
000125 (2)
000125 (6)
000125
000126 (4)
000127 (2)
000127 (6)
000127
000129 (2)
000129 (6)
000130 (4)
000131 (6)
000132 (4)
000133 (2)
000133 (3)
000134 (5)
000135 (4)
000135
000136 (4)
000136 (6)
000137 (3)
000137
000139 (4)
000139 (5)
000139 (6)
000141 (2)
000141 (4)
000142 (5)
000142 (6)
000144 (5)
000145 (6)
000146 (6)
000148 (3)
000148 (4)
000149 (4)
000151 (6)
000151
000153 (3)
000153 (4)
000153
000154 (2)
000154 (3)
000154 (4)
000155 (3)
000155
000156 (2)
000157 (6)
000158 (4)
000158 (6)
000159 (5)
000160 (4)
000162 (2)
000162
000163 (4)
000163 (5)
000163 (6)
000164 (5)
000166 (4)
000167 (2)
000168 (2)
000169 (6)
000170 (2)
000172 (6)
000174 (3)
000177 (3)

Train

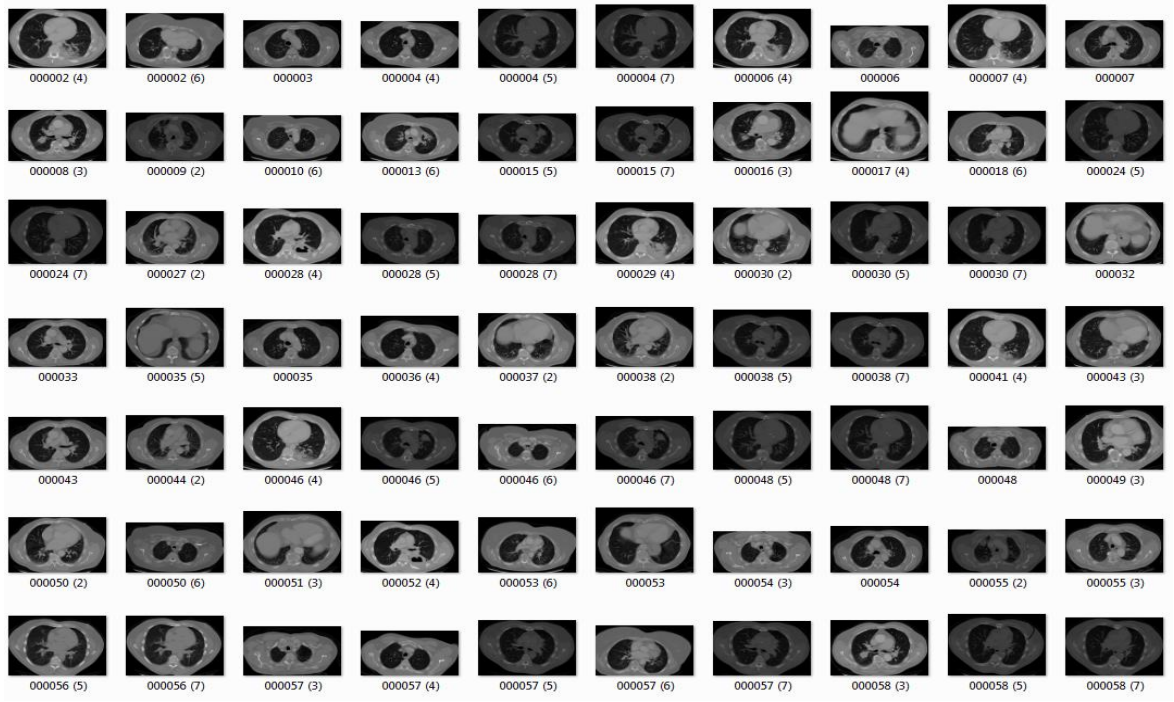
000002 (4)
000002 (6)
000003
000004 (4)
000004 (5)
000004 (7)
000006 (4)
000006
000007 (4)
000007
000008 (3)
000009 (2)
000010 (6)
000013 (6)
000015 (5)
000015 (7)
000016 (3)
000017 (4)
000018 (6)
000024 (5)
000024 (7)
000027 (2)
000028 (4)
000028 (5)
000028 (7)
000029 (4)
000030 (2)
000030 (5)
000030 (7)
000032
000033
000035 (5)
000035
000036 (4)
000037 (2)
000038 (2)
000038 (5)
000038 (7)
000041 (4)
000043 (3)
000043
000044 (2)
000046 (4)
000046 (5)
000046 (6)
000046 (7)
000048 (5)
000048 (7)
000048
000049 (3)
000050 (2)
000050 (6)
000051 (3)
000052 (4)
000053 (6)
000053
000054 (3)
000054
000055 (2)
000055 (3)
000056 (5)
000056 (7)
000057 (3)
000057 (4)
000057 (5)
000057 (6)
000057 (7)
000058 (3)
000058 (5)
000058 (7)

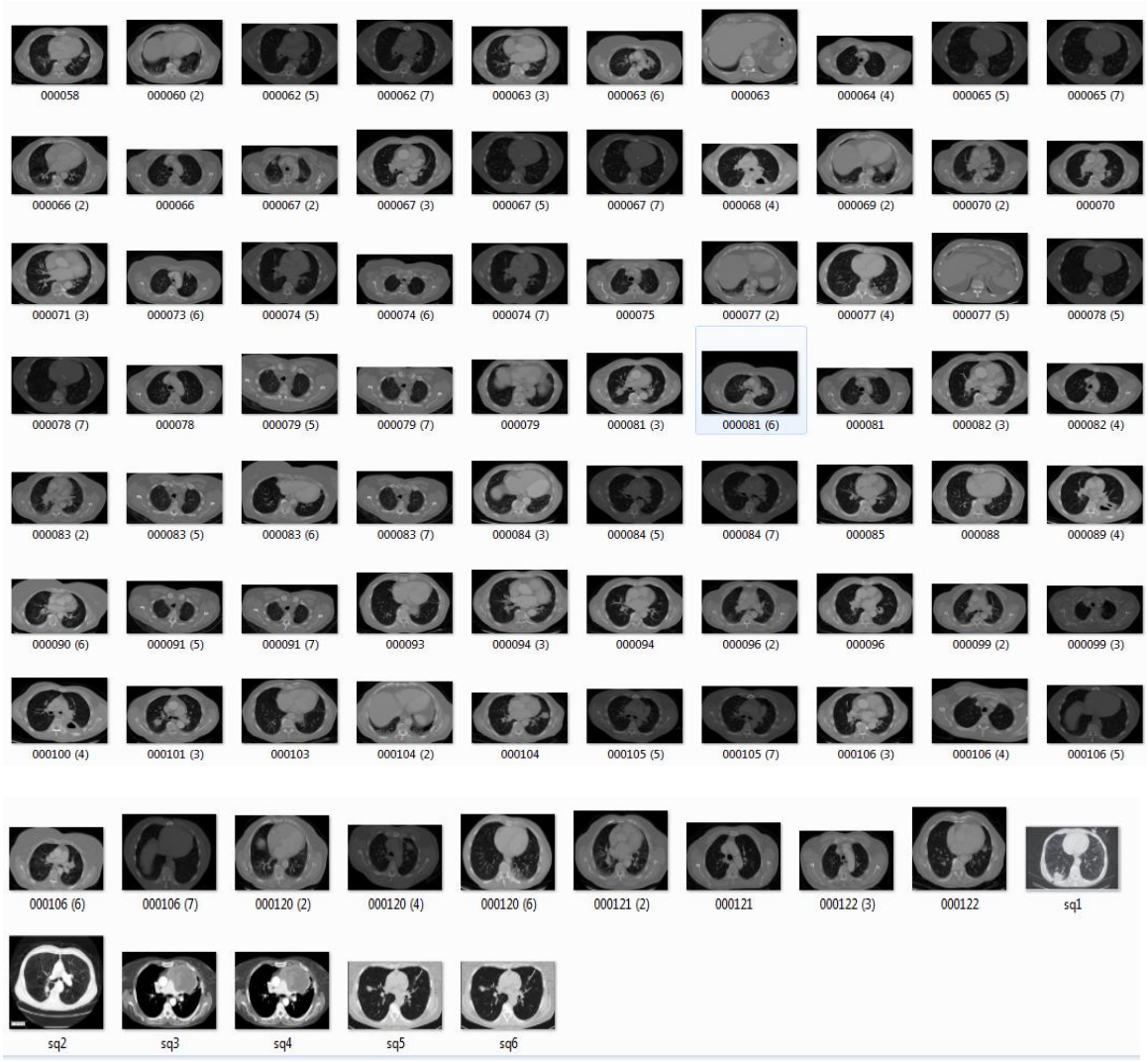

Valid

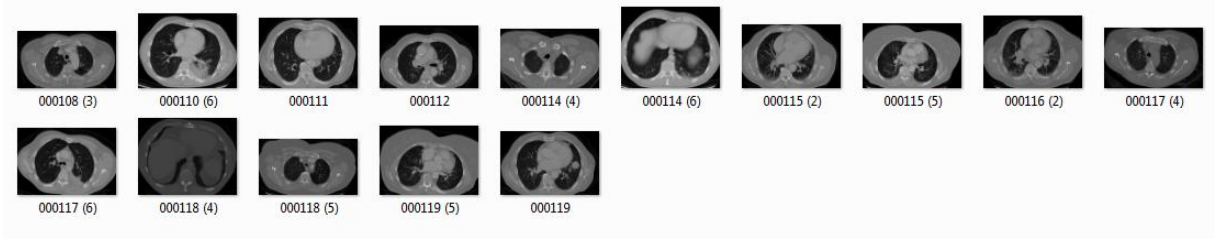

K. Simonyan and A. Zisserman of the University of Oxford proposed the VGG16 convolutional neural affiliation model in their paper "Particularly Deep Convolutional Networks for Large-Scale Image Recognition." The model accomplishes 92.7 percent top-5 test accuracy in ImageNet, a dataset of more than 14 million pictures having a spot with 1000 classes. Maybe the most surprising model entered at the 2014 ILSVRC was this one(Oueida, Aloqaily, & Ionescu, 2019). It outmaneuvers AlexNet by subbing colossal piece size channels (11 and 5 in the first and second convolutional layers, independently) with wearisome 33-piece size works with brilliantly. VGG16 had been anticipating NVIDIA Titan Black GPUs for a long time(Aloqaily, Otoum, Al Ridhawi, & Jararweh, 2019).

VGG16, which is popular due to its ease of use, is used in several deep learning image

categorization algorithms. VGG16 is frequently used in learning applications due to its benefits.

VGG16, a CNN plan, won the ImageNet Large Scale Visual Recognition Challenge (ILSVRC) in 2014. It is currently saw as potentially the most vital vision plan at whatever point planned.

VGG16 architecture

Vgg16 is 16-layer vgg architecture, as the name suggests.

During setting up, the convents are managed a fixed-size 224 by 224 RGB picture. The central pre-regulating done here is taking out every pixel's mean RGB respect from the status set. The picture is overseen utilizing a heap of convolutional (conv.) layers with channels with an incredibly confined responsive field, like 3 3 (the littlest size to get the contemplations of left/right, up/down, and focus and has an indistinguishable astounding open field as one 7 x 7). It's more tangled, with not such a huge load of cutoff concentrates yet rather more non-linearity's. In one of the plans, 1 1 convolution channels are used, which might be considered as a straight differentiation in the information channels (trailed by non-linearity). The convolution step and spatial cushioning of the conv. layer input are both set to 1 pixel for 3 x 3 convolutional layers, ensuring that the spatial target is secured later convolution. Five max-pooling layers that follow segments of the convolutional layers help spatial pooling. Stage 2 is utilized to max-pool more than a 22 pixel plan(S. Wang et al., 2020).

Three Fully-Connected (FC) layers are added later a store of convolutional layers (of affected importance in various models): the mysterious two each have 4096 channels, while the third performs 1000-way ILSVRC demand as such has 1000 channels (one for each class). The last layer is called delicate max. The completely related levels are set up the same way in all affiliations(Aichler & Walch, 2015).

All mysterious layers show the alteration (ReLU) non-linearity. Aside from one, none of the associations use Local Response Normalization (LRN), which doesn't further foster execution on the ILSVRC dataset yet extends memory use and estimation time.

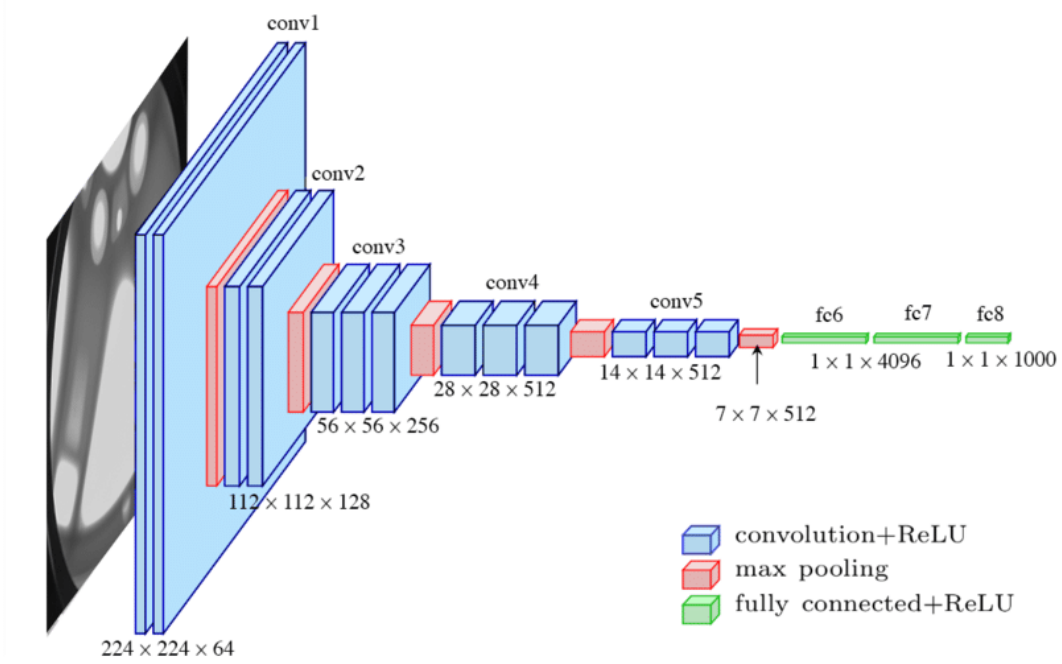

Figure 2: VGG16 architecture

Below image is a basic architecture of all 16 layers of VGG16

Vgg16_Input:Inputlayer	**Input:**	**(None,224,224,3))**
	Output:	**(None,224,224,3))**

↓

Vgg16:Functional	**Input:**	**(None,224,224,3))**
	Output:	**(None,7,7,512))**

↓

Dropout: Dropout	**Input:**	**(None7,7,512)**
	Output:	**(None,7,7,512)**

↓

Flatten: Flatten	**Input:**	**(None7,7,512)**
	Output:	**(None,25088)**

↓

Batch_Normalization:Batchnormalization	**Input:**	**(None,255088)**
	Output:	**(None,25088)**

↓

Dense:Dence	**Input:**	**(None,25088)**

	Output:	**(None,32)**

Batch_Normalization_1:Batchnormalization	**Input:**	**(None,32)**
	Output:	**(None,32)**

Activation: Activation	**Input:**	**(None:32)**
	Output:	**(None,32)**

Dropout_1:Droput	**Input:**	**(None,32)**
	Output:	**(None,32)**

Dense_1:Dense	**Input:**	**(None,32)**
	Output:	**(None,32)**

Batch_Normalization_2:Batchnormalization	**Input:**	**(None,32)**
	Output:	**(None,32)**

Activation_1: Activation:	**Input:**	**(None,32)**
	Output:	**(None,32)**

Dropout_2: Dropouts	**Input:**	**(None,32)**
	Output:	**(None,32)**

Dense _2: Dense	**Input:**	**(None,32)**
	Output:	**(None,32)**

Batch_Normalization_3:Batchnormalization	**Input:**	**(None,32)**
	Output:	**(None,32)**

Activation_2:Activation	**Input:**	**(None,32)**
	Output:	**(None,32)**

↓

Dense_3:Dense	Input:	(None,32)
	Output:	(None,4)

Results

LOSS	ACCURACY	PRECISION	RECALL	AUE	F1
1.059949756	0.77619046	0.63773594	0.30476192	0.7508273	0.406683773

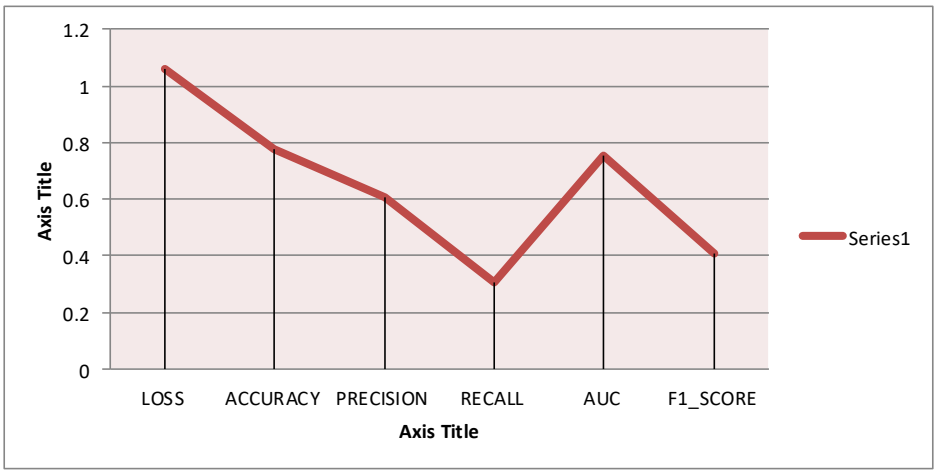

Accuracy - The easiest instinctive exhibition metric is exactness, which is only the proportion of appropriately anticipated perceptions to add up to perceptions. One would trust that assuming our model is precise, it is awesome(Chen et al., 2011). Indeed, exactness is a helpful measurement, however just when the datasets are symmetric and the upsides of bogus up-sides and bogus negatives are practically equivalent. Therefore, different boundaries should be thought of while assessing the presentation of your model. Our model got a score of 0.7762, showing that it is around 77.62 percent exact.

$$\textbf{Accuracy} = \frac{\textbf{TP} + \textbf{TN}}{\textbf{TP} + \textbf{TN} + \textbf{FP} + \textbf{FN}}$$

Precision - The proportion of precisely anticipated positive perceptions to add up to expected positive perceptions is known as accuracy. The inquiry that this action responds to is the number of the travelers who were recognized as having endure really did. The low bogus positive rate is identified with high accuracy. We have an accuracy of 0.6038, which is somewhat great.

$$\textbf{precision} = \frac{\textbf{TRUE Positive}}{\boldsymbol{True\ positive} + \boldsymbol{fales\ nagative}}$$

Recall (Sensitivity) - Indeed, review is characterized as the extent of precisely anticipated positive perceptions to all perceptions in the class. What number of the travelers who really endure were marked, as per the reactions to the inquiry? This model has a review of 0.3048, which is OK(Kuruvilla & Gunavathi, 2014).

$$\mathbf{RECALL} = \frac{\mathbf{TRue\ \ positive}}{\boldsymbol{true\ \ positive} + \boldsymbol{false\ \ nagative}}$$

F1 score - The weighted normal of Precision and Recall is the F1 Score. Thus, this score thinks about both bogus up-sides and bogus negatives. Despite the fact that it isn't so instinctive as precision, F1 is much of the time more valuable than exactness, particularly assuming the class appropriation is inconsistent. At the point when bogus up-sides and bogus negatives have identical expenses, precision functions admirably. It's ideal to take a gander at both Precision and Recall whether the expense of bogus up-sides and bogus negatives is impressively unique. The F1 score in our circumstance is 0.4067.

$$\mathbf{F1} = \frac{\mathbf{2} \times (\mathbf{precision} \ \ \times \mathbf{Recall})}{\mathbf{prcision} \ \ + \mathbf{Recall}}$$

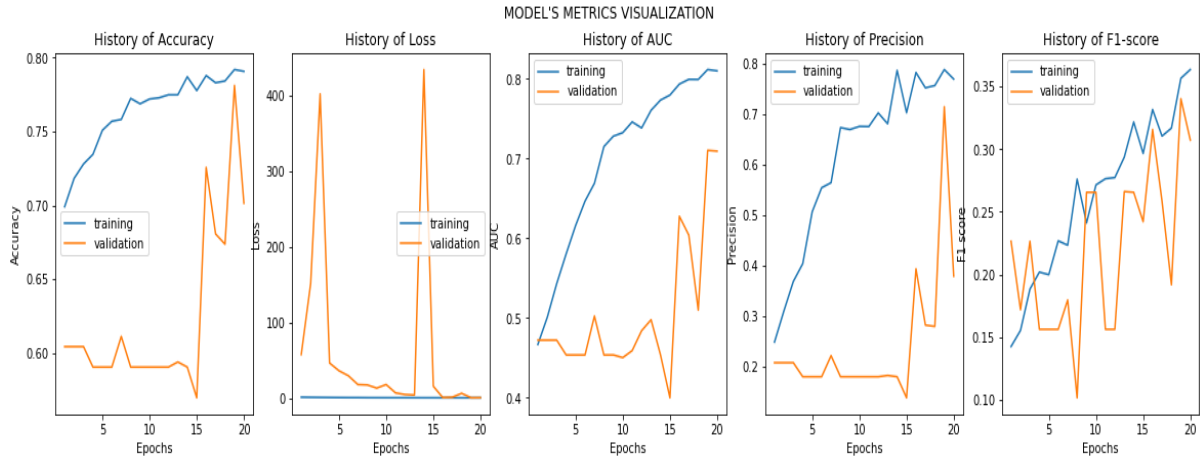

DISCUSSION

In this review, we at first incorporated an informational index of CT pictures from 125 people with beginning phase cellular breakdown in the lungs. To avoid the data set's intrinsic imbalance, revolving, shifting, and reproducing procedures are used to improve it. The VGG16 deep convolutional neural network is proposed after that. This method passes on basic execution in perceiving psychotic sorts of cell breakdown in the lungs from CT checks by using joint vote based. Significant models and aiding were utilized strangely to perceive fanatical sorts of cell breakdown in the lungs before all else periods of the sickness using little CT looks at. There are a few research avenues that could be pursued in the future. It would be interesting to enhance lung cancer typing accuracy, which may be investigated further. More contexts regarding the tumor, for example, associations with adjacent veins, just as data about the athletic patient, for example, the clinical history report, can be joined. All together for the framework to be universally relevant, future exploration might consolidate the fuse of pictures from different sources in the preparation and test datasets.

	Doctor 1	Doctor 2	Avrge of doctors	VGG16
ACCURACY	0.65	0.55	0.60	0.85
TIMES OF DIAGNOSING AN IMAGE	76s	101s	88.5s	1.3s

VGG16 and two doctors' accuracy and time costs for diagnosing 20 randomly selected C

images

CONCLUSION

This review researches the chance of data move from normal to histopathological pictures utilizing three pre-prepared organizations (VGG16) for adjusting and full-preparing.

In view of VGG16, this exploration offered another powerful CT arrangement calculation. To oblige cellular breakdown in the lungs composing, we initially made a grouping framework dependent on further developed VGG16. While testing with just 613 CT filter pictures our model can distinguish and arrange cellular breakdown in the lungs types with having a precision and time that can't be coordinated by any clinical expert with 77.61% of exactness in under 2 sec.

Future parts of this examination incorporate layer-by-layer adjusting, bigger datasets, progressed information expansion methods, (for example, contingent generative antagonistic organizations (GANs) and profound photograph style move), and different weight instatement procedures (like Xavier, He, MSRA, and Gaussian conveyance) in full organization preparing.

Finally, we can conclude that ultrasound is an effective diagnostic tool for endometriosis. To enhance its effectiveness, more research is needed in order to measure the sensitivity and specificity of different imaging modalities such as Ultrasound or MR scans.

REFERENCES

Aichler, M., & Walch, A. (2015). MALDI Imaging mass spectrometry: current frontiers and perspectives in pathology research and practice. *Laboratory investigation, 95*(4), 422-431.

Aloqaily, M., Otoum, S., Al Ridhawi, I., & Jararweh, Y. (2019). An intrusion detection system for connected vehicles in smart cities. *Ad Hoc Networks, 90*, 101842.

Barbareschi, M., Cantaloni, C., Del Vescovo, V., Cavazza, A., Monica, V., Carella, R., . . . Silvestri, M. (2011). Heterogeneity of large cell carcinoma of the lung: an immunophenotypic and miRNA-based analysis. *American journal of clinical pathology, 136*(5), 773-782.

Barnes, L., Eveson, J., Reichart, P., & Sidransky, D. (2005). World Health Organization classification of tumours: pathology and genetics of head and neck tumours.

Chang, J. C., & Kundranda, M. (2017). Novel diagnostic and predictive biomarkers in pancreatic adenocarcinoma. *International journal of molecular sciences, 18*(3), 667.

Chen, H., Wu, W., Xia, H., Du, J., Yang, M., & Ma, B. (2011). *Classification of pulmonary nodules using neural network ensemble.* Paper presented at the Advances in Neural Networks–ISNN 2011: 8th International

Symposium on Neural Networks, ISNN 2011, Guilin, China, May 29–June 1, 2011, Proceedings, Part III 8.

Kundu, S., Mitra, R., Misra, S., & Chatterjee, S. (2012). Squamous cell carcinoma lung with progressive systemic sclerosis. *The Journal of the Association of Physicians of India, 60*, 52-54.

Kuruvilla, J., & Gunavathi, K. (2014). Lung cancer classification using neural networks for CT images. *Computer methods and programs in biomedicine, 113*(1), 202-209.

Nawa, T., Nakagawa, T., Mizoue, T., Kusano, S., Chonan, T., Fukai, S., & Endo, K. (2012). Long-term prognosis of patients with lung cancer detected on low-dose chest computed tomography screening. *Lung Cancer, 75*(2), 197-202.

Oueida, S., Aloqaily, M., & Ionescu, S. (2019). A smart healthcare reward model for resource allocation in smart city. *Multimedia tools and applications, 78*, 24573-24594.

Siegel, R. L., Miller, K. D., & Jemal, A. (2015). Cancer statistics, 2015. *CA: a cancer journal for clinicians, 65*(1), 5-29.

Travis, W. D., Rekhtman, N., Riley, G. J., Geisinger, K. R., Asamura, H., Brambilla, E., . . . Powell, C. A. (2010). Pathologic diagnosis of advanced lung cancer based on small biopsies and cytology: a paradigm shift. *Journal of thoracic oncology, 5*(4), 411-414.

Wang, A., Wang, H., Liu, Y., Zhao, M., Zhang, H., Lu, Z., . . . Liu, G. (2015). The prognostic value of PD-L1 expression for non-small cell lung cancer patients: a meta-analysis. *European Journal of Surgical Oncology (EJSO), 41*(4), 450-456.

Wang, S.-H., Zhang, Y.-D., Yang, M., Liu, B., Ramirez, J., & Gorriz, J. M. (2019). Unilateral sensorineural hearing loss identification based on double-density dual-tree complex wavelet transform and multinomial logistic regression. *Integrated Computer-Aided Engineering, 26*(4), 411-426.

Wang, S., Sun, J., Mehmood, I., Pan, C., Chen, Y., & Zhang, Y. D. (2020). Cerebral micro-bleeding identification based on a nine-layer convolutional neural network with stochastic pooling. *Concurrency and Computation: Practice and Experience, 32*(1), e5130.

Wei, X., Guo, G., Wang, H., & Wan, H. (2015). *A multiscale method for HOG-based face recognition.* Paper presented at the Intelligent Robotics and Applications: 8th International Conference, ICIRA 2015, Portsmouth, UK, August 24-27, 2015, Proceedings, Part I 8.

Wiener, R. S., Schwartz, L. M., Woloshin, S., & Welch, H. G. (2011). Population-based risk for complications after transthoracic needle lung biopsy of a pulmonary nodule: an analysis of discharge records. *Annals of internal medicine, 155*(3), 137-144.